

## X-RAY DIFFRACTION STUDY OF STRUCTURE OF CaO—Al<sub>2</sub>O<sub>3</sub>—SiO<sub>2</sub> TERNARY COMPOUNDS IN MOLTEN AND CRYSTALLINE STATES

V.E. Sokol'skii <sup>a</sup>, D.V. Pruttskov <sup>b</sup>, O.M. Yakovenko <sup>a</sup>, V.P. Kazimirov <sup>a</sup>, O.S. Roik <sup>a</sup>,  
N.V. Golovataya <sup>a</sup>, G.V. Sokolsky <sup>c</sup>

<sup>a</sup> Taras Shevchenko National University of Kyiv, Ukraine

<sup>b</sup> ZAO «Tekhnokhim», Zaporozhye, Ukraine

<sup>c</sup> National Technical University of Ukraine "Igor Sikorsky Kyiv Polytechnic Institute"

(Received 06 August 2019; accepted 29 June 2020)

### Abstract

Anorthite and gehlenite crystalline structure and short-range order of anorthite melt have been studied by X-ray diffraction in the temperature range from room temperature up to ~ 1923 K. The corresponding anorthite and gehlenite phases were identified as well as amorphous component for anorthite samples having identical shape to XRD pattern of the anorthite melt. The structure factor and the radial distribution function of atoms of the anorthite melt were calculated from the X-ray high-temperature experimental data. The partial structural parameters of the short-range order of the melt were reconstructed using Reverse Monte Carlo simulations.

**Keywords:** Gehlenite; Anorthite; Mullite; High-temperature X-Ray diffraction; RMC simulations

### Abbreviations

IC is the intensity curve of X-Ray diffraction  
SF - the structure factor  
RDF - the radial distribution function  
RMC - the reverse Monte-Carlo method  
CN - the average coordination number of atoms  
ASNG - the alumina silicate nanogrouping  
CAS - CaO—Al<sub>2</sub>O<sub>3</sub>—SiO<sub>2</sub> system  
R<sub>i</sub>(i-j) the most probable nearest interatomic distances between atoms of i- and j-type.

### 1. Introduction

Materials based on the CaO—Al<sub>2</sub>O<sub>3</sub>—SiO<sub>2</sub> (CAS) and MgO—Al<sub>2</sub>O<sub>3</sub>—SiO<sub>2</sub> ternary diagrams are crucial for the Ukrainian national economy and other countries due to numerous applications. For example, slags based on these systems are applied in blast furnace production. Many welding fluxes and fluxes for surfacing are also known [1]. Gehlenite, anorthite, mullite, sillimanite, and other synthetic compounds of the CAS system have been used at ZAO "Technohim" (Zaporizhia, Ukraine).

It should be noted that the number of publications about the properties and structure of the main minerals of this system in liquid and crystalline states are relatively limited [2-6]. We performed

investigation of the melts of three eutectic CAS oxide system samples [6] by high-temperature X-ray diffraction. The study of the ceramic welding flux based on the MgO—Al<sub>2</sub>O<sub>3</sub>—SiO<sub>2</sub> system with CaF<sub>2</sub> additives are presented in [7]. In accordance with [6] the eutectics exist at the anorthite region boundaries.

Our previous high-temperature study [6] allows concluding that the anorthite is present in all solid samples of the eutectics. The present work is devoted to the investigation of anorthite and gehlenite compositions which are only known as the ternary compounds of the CAS system. The study of anorthite and gehlenite both in solid and molten states is necessary to understand the nature of the interaction in the CAS system, since the minerals that are formed are very important for physical chemistry, metallurgy, and materials science.

### 2. Experimental procedure

At the initial stage, the powders of Al<sub>2</sub>O<sub>3</sub>, SiO<sub>2</sub>, and CaCO<sub>3</sub> reagents of especially pure grade were mixed in required ratios and were grounded by "Retsch PM 400" ball mill. The ternary compounds were synthesized by heat treatment in the platinum-iridium alloy crucibles at 1750°C for 2 h using the Tamman furnace in the flow of high purity argon with further cooling to room temperature (RT). The cores

\*Corresponding author: sokol@univ.kiev.ua



of the samples were separated from the crucibles without touching the crucibles walls using diamond-coated drill. The resulting product was ground again in the same mill and then was further purified in a laboratory scale magnetic separator. Composition, melting points, experimental temperature, and phase composition before melting according to XRD analysis are shown in Table 1.

**Table 1.** Composition, melting points, investigated temperatures, and phase composition of investigated samples

№	Composition, atomic fraction			Melting point, K	Temperatures of investigation, K	Phase composition before melting
	CaO	Al <sub>2</sub> O <sub>3</sub>	SiO <sub>2</sub>			
1	0.25	0.25	0.5	1820 [8] 1873 [our data]	293(RT), 1073, 1273, 1373, 1473, 1673, 1773, 1873 (melt)	CaAl <sub>2</sub> Si <sub>2</sub> O <sub>8</sub>
2	0.5	0.25	0.25	1863 [8]	293 (RT), 773, 1073, 1273, 1473, 1673	Ca <sub>2</sub> Al <sub>2</sub> SiO <sub>7</sub>

The powdered sample was placed in a special molybdenum (Mo) crucible with the carefully smoothed out and polished inner surface to reduce the interaction with the investigated melts. The XRD study was performed by a high-temperature X-ray  $\theta$ - $\theta$  diffractometer using monochromatic MoK $\alpha$  radiation in a vacuum chamber filled with high-purity helium X-ray diffractometer. The design and experimental procedure of the diffractometer were described in [2,6,9,10]. The XRD pattern of anorthite at room temperature is shown in Fig. 1. The amorphous backgrounds of the XRD patterns of the anorthite at all investigated temperatures are shown in Fig. 2. The crystalline part of the XRD patterns of anorthite at

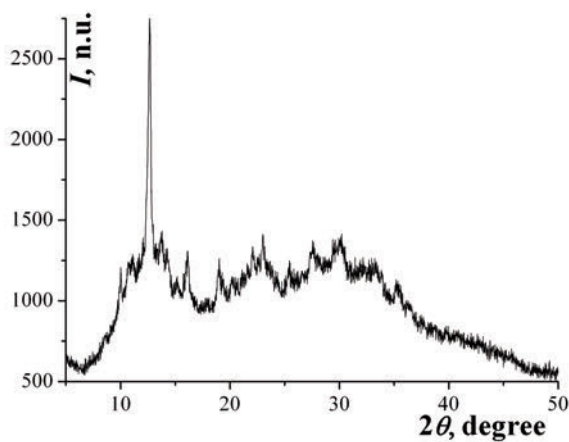


**Figure 1.** XRD pattern of anorthite at room temperature

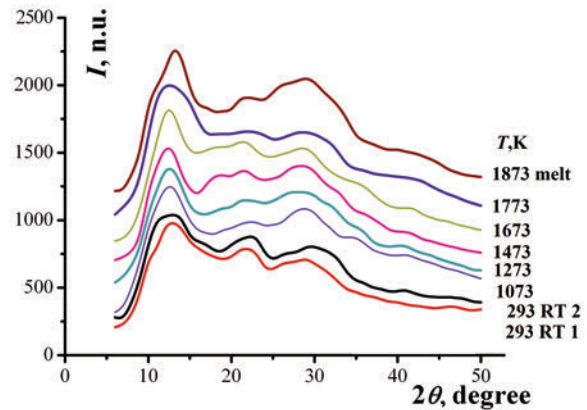


**Figure 2.** Normalized background of anorthite sample in liquid and solid states at different temperatures. There are two curves at RT: before (1) and after remelting (2)

different temperatures in comparison with the XRD of the anorthite melts are given in Fig 3. After amorphous background subtraction the all XRD patterns were normalized to maximum intensity of 1000 n.u.

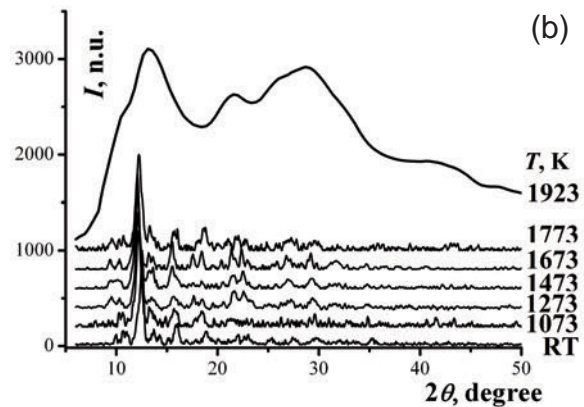
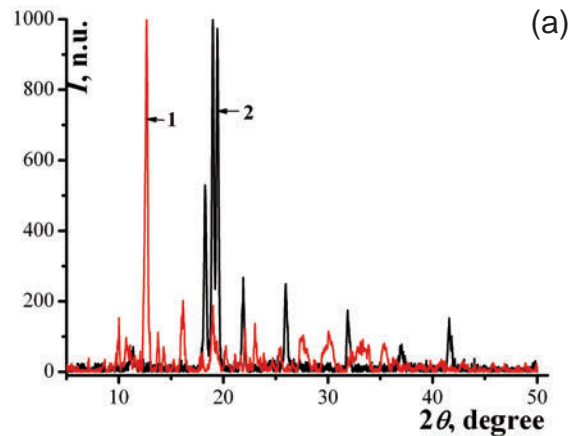


**Figure 3.** XRD patterns of crystalline anorthite at different temperatures (a) and anorthite melts (above); XRD patterns of anorthite at room temperature (b) before (1) and after remelting (2)

The XRD patterns of gehlenite at various temperatures are shown in Fig. 4 and 5. The subtraction of the amorphous background and normalization of the XRD patterns of gehlenite were performed in the same way as in the anorthite case. The following software was applied to analyze crystalline diffraction patterns: PCW, Match, X'Pert HighScore Plus, and Diamond 3.2.

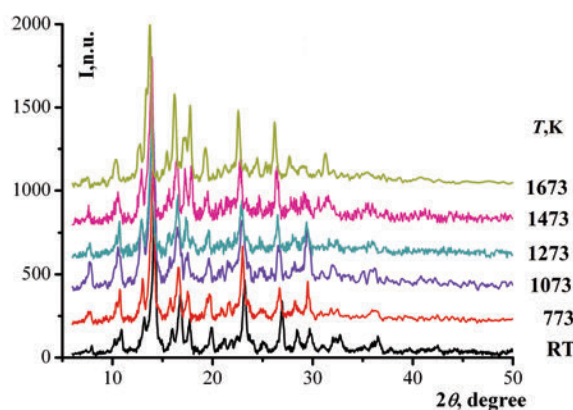


Figure 4. X-Ray patterns of gehlenite samples at different temperatures

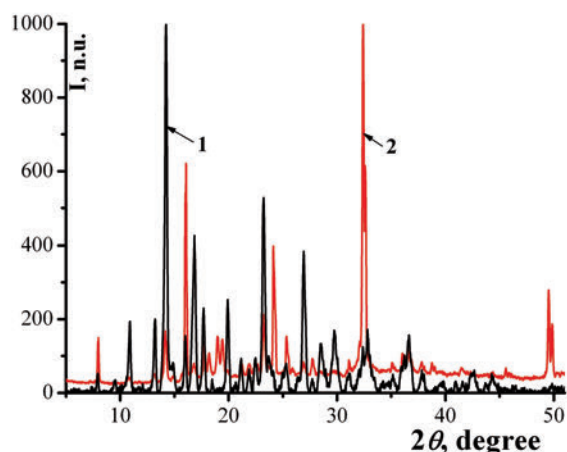


Figure 5. XRD patterns of gehlenite samples at room temperature before (1) and after remelting (2)

The phase diagram of CAS system is shown in Fig. 6. The red circles indicate the location of the ternary compounds that are studied in this work. The gray circles show the compositions (1,2,3) investigated in [6]. It should be noted that the anorthite position on CAS phase diagram is in the immediate vicinity of the mullite field, and gehlenite is much further. Therefore, the composition of the sample studied in [4] (green circle) is even more enriched with calcium oxide and having structure in the molten state that may differ significantly.

The XRD-pattern of molten anorthite at 1923 K

was obtained by high-temperature  $\theta$ - $\theta$  diffractometer (MoK $\alpha$  radiation). It should be noted that the anorthite melting point is in accordance with [8]. However, the XRD pattern of anorthite sample at 1820 K contains unstable crystalline peaks which do not match with mullite phase. The completely molten sample was obtained at 1873 K only. Nevertheless, the experimental temperature was increased up to 1923 K to avoid the mentioned unstable effects observed near the melting point.

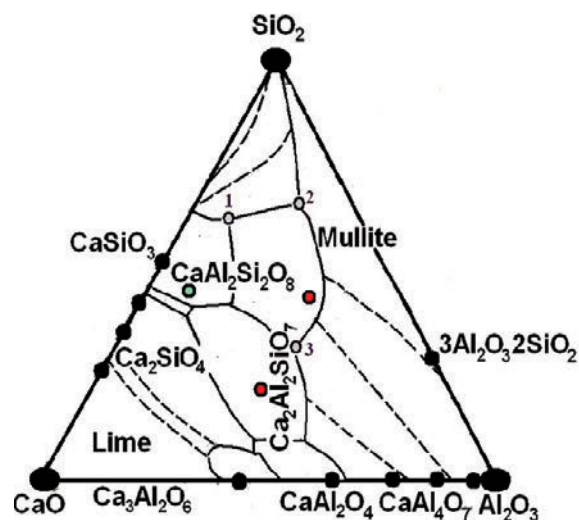


Figure 6. Phase diagram of the CAS system. The investigated ternary compound (red circle), the eutectic samples (1,2,3) studied in [6] (gray circles)

The structure factor (SF) and the radial distribution function (RDF) curves were calculated by self-developed software [6,7]. The structure models were reconstructed from the experimental data (experimental SF) using Reverse Monte Carlo (RMC) simulations [11,12,13]. There are no experimental

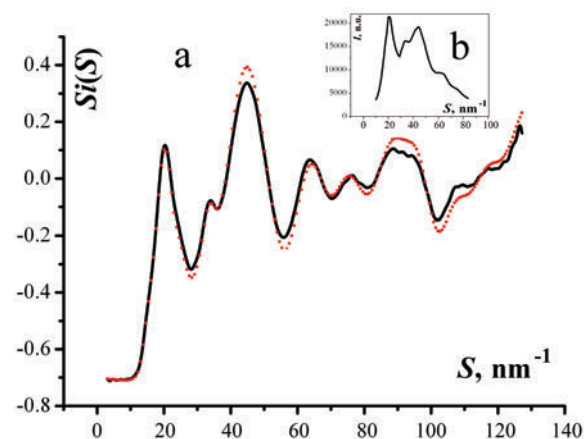


Figure 7. Experimental (solid line) and simulated (dotted line) SF (a) and experimental IC (b) for anorthite melt

densities of the CAS melts; therefore, the required melt density values at the investigated temperature were evaluated using the approach proposed in [14]. This method is based on the analysis of the RDF region before the first (main) peak. It allows estimating adequate density values of the investigated melts. Fig. 7, 8 show the SF and RDF curves for the anorthite melt. The dotted line in Fig. 7a is the SF curve obtained by RMC simulations, the solid line – experimental data. The experimental and simulated structure factor curves are consistent and complement each other within the experimental error.

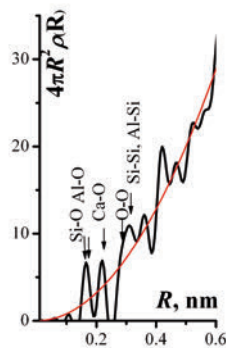


Figure 8. Radial distribution curve for the anorthite melt

### 3. Results

#### 3.1 Crystalline samples

The XRD pattern of anorthite samples at RT and annealed at different temperatures contain reflections identified as crystalline anorthite phase as well as the rather strong background of the amorphous component. An example of such XRD pattern at RT is shown in Fig.1. The amorphous contributions at all experimental temperatures are presented in Fig.2. These patterns have a certain similarity with each other and resemble a scattering curve from the melt. Therefore, it might lead to the preliminary conclusion that the crystalline and amorphous components have the identical composition in the samples. The reflexes of different XRD patterns of crystalline anorthite sample (up to 1773 K) were identified as the anorthite phase. The good agreement with the peaks positions with minor differences in the peaks relative intensities were observed. There were no changes up to the melting point with the exception of an enlargement of the anorthite phase lattice parameters with the temperature rise and the characteristic intensive amorphous background of the anorthite XRD patterns. During the solidification of the remelted sample in the furnace cooling mode there is not enough time to form crystalline phases; therefore, an amorphous phase is also formed (Fig.1). It should be noted that both crystalline and non-crystalline scattering components have no changes even during

the long isothermal treatment. The anorthite sample XRD pattern was changed significantly (Fig. 3b) after melting and heat treatment for two hours at 1923 K and following fast cooling in accordance with the furnace cooling mode. It may be noted that after the remelting the XRD of the solid sample has weak peaks of the anorthite phase and more intense peaks of the unidentified phase (phases) that was absent before melting. The non-crystalline component of the scattering is very high and remains practically the same after melting (Fig. 2).

The amorphous background is practically absent on the XRD patterns of gehlenite (Fig. 4) (unlike the XRD patterns of anorthite). The temperatures of this study are indicated in Table. 1 and Fig. 4. The melting point of gehlenite is 1866 K [8]. Unfortunately, our attempts to register a typical liquid curve were failed up to the temperatures of about 1700°C (the limiting operating of a high temperature diffractometer). The XRD patterns of the gehlenite samples were interpreted as a gehlenite phase below the melting point (up to 1773 K). The background amorphous component is practically absent before and after melting on the diffractograms. Like anorthite, the crystalline component undergoes significant changes after remelting. To interpret the obtained data successfully we should assume that the gehlenite (and probably anorthite) partial decomposition into simple oxides and more complex  $\text{CaSiO}_3$  type double oxides have a place. The absence of amorphous background on XRD pattern of the gehlenite can be explained by difference of their melt viscosity ( $2.5 \text{ Pa}\cdot\text{s}$  for anorthite and  $0.27 \text{ Pa}\cdot\text{s}$  for gehlenite melts) [17]. In case of the anorthite, the crystallization is complicated by higher viscosity of the corresponding melt; therefore, the amorphous phase is formed.

#### 3.2. RDF analysis of the anorthite melt

The first maximum on the experimental RDF has a position at 0.167 nm. According to our data, it can be the superposition of Si-O (0.164 nm) and Al-O (0.169 nm) coordination contributions. Silicon and aluminum coordination numbers by oxygen were calculated by the formula:

$$A_{\text{Si}(O)} = 2n_{\text{Si}}K_{\text{Si}}K_{\text{O}}Z_{\text{Si}(O)}eA_{\text{Al}(O)} = 2n_{\text{Al}}K_{\text{Al}}K_{\text{O}}Z_{\text{Al}(O)} \quad (1)$$

where  $A_{\text{Al}(O)}$  and  $A_{\text{Si}(O)}$  are the areas of Gaussian curves (coordination contributions) calculated from experimental RDF,  $n_{\text{Me}}$  is the atomic fraction of the corresponding oxide component;  $K_{\text{Me}}$ ,  $K_{\text{O}}$  are the atomic scattering factors of elements averaged out at scattering angles and composition,  $Z_{\text{Me}(O)}$  is the coordination number (CN) of silicon or aluminum by oxygen. The Equation (1) describes the case of central cationic polyhedron surrounded by polyhedrons of the



same type. So far as the atomic fractions and scattering factors ( $K_{Me}$ ) are slightly different, they give very similar results. The oxygen polyhedrons with silicon and aluminum atoms inside (mostly tetrahedra) form joint nanogroupings. These aluminosilicate nanogrouping (ASNG) based on the close packed structure of oxygen atoms with  $Al^{3+}$  occupying both octahedral and tetrahedral sites,  $Si^{4+}$  occupying tetrahedral ones that form in the molten and amorphous states.

Calcium atoms are probably not a part of such groupings. The coordination contribution of Ca-O is observed at 0.223 nm (the position of the peak  $R_1(Ca-O) = 0.223$  nm) and the calcium coordination number by oxygen is quite large (about 9.5). This value of coordination number is undoubtedly too large to support joint Si-Al-Ca-O nanogroupings since the octahedral cavities formed in close packed ASNG will be small to accommodate  $Ca^{2+}$  cations. According to the obtained data, the melt consists of Si-Al-O nanogroupings with calcium cations concentrated on the surface of the ASNG and followed by the outer layer of oxygen atoms.

### 3.3 RMC simulations of the anorthite melt

The simulated SF is in good agreement with the experimental one (Fig 7). It may be noted that unlike most oxide melts the first maximum on SF is lower than the second one. The structural parameters obtained by both RDF and RMC methods correlate well with each other. For example, according to RDF analysis the  $R_1(Si-O)$  is 0.164 nm and  $R_1(Al-O)$  is 0.169 nm. The closest interatomic  $R_1(Si-O)$  and

$R_1(Al-O)$  distances obtained from the partial pair correlations functions (RMC data) are equal to 0.163 and 0.171 nm, respectively (Fig. 9, a1). The corresponding CNs for both cases are close to 4 (Fig. 9, a2). Therefore, four oxygens are coordinated predominantly around the silicon or aluminum atom. The distance of  $R_1(Ca-O)$  is equal to 0.219 nm (Fig.9, a1), CN = 8.7 (Fig.9, a2). This value is slightly lower than the one calculated from the RDF (9.5 atoms) but it is still high. Fig. 9, a2 shows also the partial pair correlation functions ( $g_{ij}(r)$ ) for Al-Al and Si-Si bonds that are very similar to each other although not clearly expressed. In both cases the position of the first peak is close to 0.314 nm ( $R_1(Al-Al)$  and  $R_1(Si-Si)$  are 0.314 nm). Partial  $g_{AlSi}(R)$  resembles  $g_{AlAl}(R)$  and  $g_{SiSi}(R)$ , however, the  $R_1(Al-Si)$  is somewhat larger (~ 0.318 nm). The similarity of  $g_{AlSi}(R)$ ,  $g_{AlAl}(R)$  and  $g_{SiSi}(R)$  is probable due to  $Al^{3+}$ ,  $Si^{4+}$  ions occupying the same positions in the ASNG. According to the results of [6], the eutectic melts are characterized by the CN of aluminum by oxygen is between 4.3 and 5.3 [6], confirming 5-6 oxygen atoms surrounding aluminum. In the present work, the RDF calculation estimates  $Z_{Al(O)}$  as ~ 4.05, and RMC provides ~ 3.9. Therefore, both methods indicate that almost all aluminum cations (like silicon) are in the oxygen tetrahedron centre.

Aluminum (or silicon) atoms are surrounded by ~2 atoms of the same kind and ~2 atoms of the different kind (Si or Al, consequently). It is assumed that the low value of CN is caused by the bonds of non-bridge oxygen with the  $Ca^{2+}$  on the surface of the ASNG as a part of the oxygen surroundings of silicon and aluminum cations. If aluminum and silicon

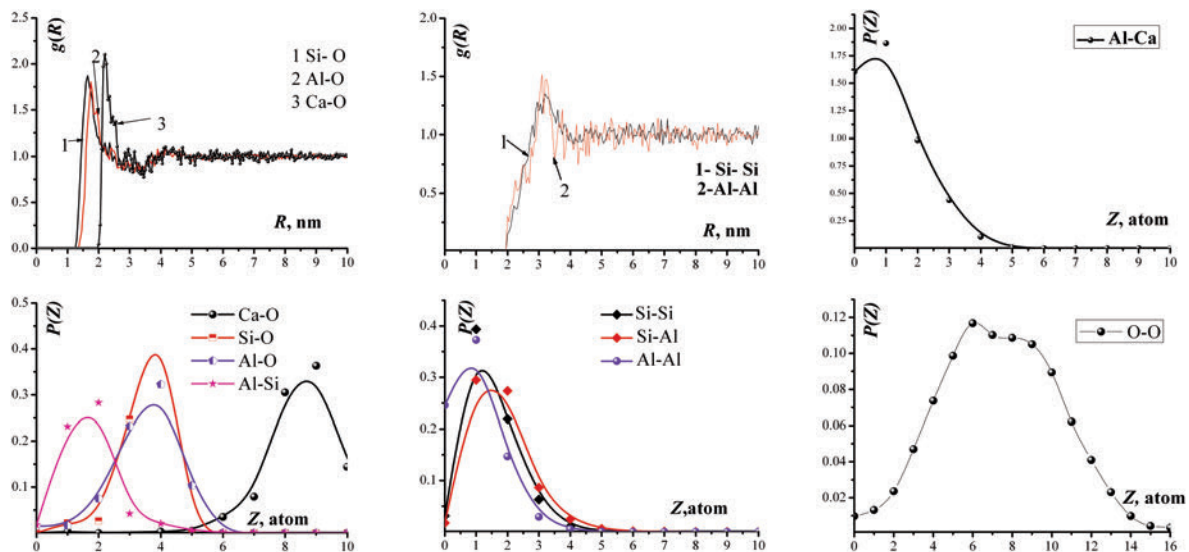


Figure 9. Partial pair correlation functions  $g_{ij}(R)$  and coordination number distributions  $P(Z)$  calculated from RMC-model of the anorthite melt:  $g_{SiO}(R)$ ,  $g_{SiO}(R)$ ,  $g_{SiO}(R)$  (a1),  $g_{SiAl}(R)$ ,  $g_{SiSi}(R)$  (b1),  $Z_{Al(Ca)}$  coordination distribution (c1),  $Z_{Ca(O)}$ ,  $Z_{Si(O)}$ ,  $Z_{Al(O)}$  and  $Z_{Al(Si)}$  coordination distribution (a2),  $Z_{Si(Si)}$ ,  $Z_{Al(Al)}$ , and  $Z_{Al(Si)}$  (a2),  $Z_{O(O)}$  coordination distribution (c2)



cations were in oxygen tetrahedral microregions (which may occur in some crystals),  $Z_{Al(AI)}$  and  $Z_{Si(Si)}$  CNs would be close to 4, and  $Z_{Ca(AI)}$  and  $Z_{Ca(Si)}$  would be about zero ( $\sim 1$  according to RMC method). Figure 9 c1 shows that the aluminum cation surrounding includes approximately one  $Ca^{2+}$ , and less than one  $Ca^{2+}$  is coordinated around silicon (not shown in the figure). The obtained results support the indication of the presence of the ASNG in the melt.

The  $g_{oo}(R)$  has main maximum at 0.275 nm, which is characteristic of  $R_1(O-O)$  distance in the grid of silicon-oxygen tetrahedrons, but it is somewhat shorter than in the aluminium-oxygen tetrahedron. Obviously, a slightly longer distance is also characteristic for  $AlO_4$  tetrahedron. In our opinion, a small influx  $g_{oo}(R)$  in the region of 0.32 nm is typical for  $R_1(O-O)$  in calcium polyhedrons (not shown in the figures). The  $Z_{O(O)}$  coordination distribution is broad (Fig. 9, c2) and demonstrates a significant contribution of large coordinations. The small  $Z_{O(O)}$  contribution could be from the ASNG, while the large one forms the nearest oxygen surroundings of  $Ca^{2+}$ .

The obtained  $Z_{Ca(O)}$  values (between 8 and 12) is overestimated in contrary to  $Z_{Ca(O)}$  values close to 6 in slag melts [6-7]. The model of multicomponent silicate melt structure based on close packed shell of oxygen atoms, with all the cations of the melt occupying the existing tetrahedral and octahedral cavities, was also proposed in [9]. Smaller cations are located closer to the center of this grouping, whereas larger cations are closer to the periphery. However, such a model is unsuitable for the investigated melt and the eutectic melts [6]. In this study, the melt structure model of the same system is proposed close to the mullite existence region. It has been assumed that thermally stable ASNG are formed in the melt. However, these nanogroups are different than mullite-sillimanite type nanogroupings. As shown in [6], the negative surface charge of oxygen layer on the boundary of the nanogrouping is neutralized by  $Ca^{2+}$  cations. These cations form a positively charged surface layer around the ASNG, which in turn is surrounded by oxygen atoms in the melt.

The mullite-sillimanite type ASNG (close spherical shape) are based on the close packed oxygen atoms, whose tetrahedral cavities (according to our data) can be occupied with silicon or aluminum atoms, with some octahedral cavities filled by aluminum atoms. In anorthite type melts, the low CN of aluminum cations ( $\sim 4$ ) and other data indicate that aluminum cations are predominantly tetrahedrally surrounded by oxygen. By the way, the sample 1 in [6] (see Fig.6), whose composition is the most distant from the phase mullite region, is characterized by the smallest CN  $Z_{Al(O)} \sim 4.1-4.5$ . In melt 2 (see Fig.6)  $Z_{Al(O)}$  is 4.4-5.3, and  $Z_{Al(O)}$  is  $\sim 4.9-5.1$ . In our opinion, six oxygen-coordinated  $Al^{3+}$ , in the anorthite melt, can

only be in a disordered quasi-gas matrix, in which the ASNG are also located. This matrix is highly disordered and makes an insignificant contribution to scattering. Therefore, groupings based on  $AlO_6^{3-}$  are not observed. The expansion of nanogrouping size with temperature increasing can lead to diffusion of aluminum atoms into the expanding octahedral vacant positions. Calcium cations with significantly larger size compared to aluminum and silicon will be forced to occupy positions outside of the ASNG.

#### 4. Discussion

Crystalline anorthite can be attributed to framework aluminosilicates (Fig. 10, a1). Alternating layers of pure aluminosilicate tetrahedra and layers that have cavities saturated with calcium cations exist in the crystalline structure anorthite. Figure 10, b1 shows a fragment of the the anorthite unit cell in the form of coordination polyhedrons. As can be seen in Fig. 10, b1, all Si (yellow) and Al (green) polyhedrons are tetrahedral, and calcium polyhedrons consist of irregular polyhedrons of complex shape with CN of about 8-9. Tetrahedrons are linked by vertices, but calcium cation polyhedrons have no bonds with one another. The part of  $SiO_4$  and  $AlO_4$  tetrahedrons are connected with  $Ca^{2+}$  polyhedrons even by faces.

Mullite also belongs to framework aluminosilicates, forming infinite 3D-grid of aluminum-silicon-oxygen tetrahedrons in crystalline state. However, it contains aluminum-oxygen octahedron groupings, with aluminum atoms playing the role of cations. The fragment of mullite structure is shown in Fig. 10, c2 (all atoms outside polyhedrons were removed). The  $SiO_4$  and  $AlO_4$  tetrahedrons and  $AlO_6$  octahedrons are highlighted here in orange and green, respectively. Crystalline mullite reflections (hardly distinguishable from the liquid melt curve) were observed for all the melts investigated in [6]. Therefore, it can be suggested that mullite type ASNG are formed in the samples near the melting point in the present work. However, this suggestion was not confirmed by subsequent analysis. The predominant tetrahedral oxygen cations of aluminum and the presence of calcium cations around the ASNG significantly distinguish the structure of the anorthite melt from the mullite one. Calcium cations were present in all eutectic compositions in [6]; however, the ASNG in the anorthite and mullite melts significant differences. In anorthite and, possibly, in melt 1 from ref. [6] (Fig.6), the silicon and aluminum cations occupy mainly the positions inside the tetrahedron of oxygen atoms, and in melts close to mullite region, aluminum cations partially occupy octahedral positions.

Assuming that the substance will retain some similarity with its high-temperature crystal structure



after melting we should expect some specific features of the crystal remaining in the melt. The obtained data allow suggesting that the ASNG have the anorthite type in case of the investigated melt and the melt 1 from ref. [6]. The mullite type of nanogrouping has place for sample 2 and 3 [6] (Fig.6). In contrary to [6], the crystalline mullite peaks were not observed in the investigated melts in anorthite type melt before and after melting, although probably some peaks (at least two in Fig. 3b) can be interpreted as mullite after remelting. Like [6] this paper supports the suggestion of the presence of the ASNG, with their negative surface charge neutralized by calcium cations. Nevertheless, the ASNG of the investigated melts have some differences from the ASNG of the melts investigated in [6]. The ASGN in the anorthite melt have practically empty octahedral cavities. On the other hand, a significant part of the octahedral cavities contains aluminum atoms in the melts close to the mullite phase region.

According to [8] the complex aluminosilicate particle existence transferred to an anode and  $\text{Ca}^{2+}$  ions migrating to a cathode in the anorthite melt. Johnson et al. [15] indicated that there are two types of oxygen ions in supercooled silicate melts (bridging and non-bridging). Bridging oxygens form bonds with two grid-forming cations, whereas non-bridging oxygens are associated with only one grid-forming cation. In accordance with [6], the contributions of non-crystalline and crystalline components should be established from the diffraction data obtained for anorthite before melting in the investigated temperature range. The non-crystalline component is represented by strongly disordered ASNG resembling the melt structure. The crystalline part consists of anorthite polycrystals. In general, after melt the solidification crystals of the same type as before melting are usually obtained. The ASNGs formed during melting mainly retain other microgroupings in the nearest surroundings. They rapidly restore bond distances with one another and build a long-range order during solidification. However, in high viscosity melts, some particles that pass significant diffusion distances have no time to occupy their crystal lattice positions during fast cooling. They can interact with one another forming more simple compounds. Therefore, anorthite and gehlenite can decompose, and, as a result, their decomposition products are observed. Applying the high-temperature microscopy method, Welch et al [16] observed the appearance of corundum crystals and pseudovollastonite  $\text{CaSiO}_3$  upon cooling the anorthite melt from 1873 to 1673 K, although the remaining part of cooled sample consisted of various modifications of anorthite. Berezhnoi [8] suggested partial decomposition of anorthite during melting but appearance of corundum was explained by non-equilibrium (fast)

crystallization of the melt.

In our opinion, the crystalline part of anorthite is completely transformed into a melt structure upon melting. The non-crystalline part is also reconstructed but insignificantly since the non-crystalline SRO in many respects resembles a liquid one. At least at the initial stage, a homogeneous liquid structure of the anorthite melt is formed. Although crystalline peaks are still observed in the anorthite melt, they are unstable and not close to mullite as shown in [6]. These peaks disappear after overheating and long exposures at high temperatures. Unfortunately, these peaks could not be interpreted since their instability during the XRD experiment.

In accordance with the proposed model, the ASNG are formed inside of a disordered (quasi-gas) matrix in the anorthite type melt. The molten matrix consists of atoms and small atomic clusters which have a weak interaction and diffusion equilibrium with each other. The molten matrix interaction forces with the ASNG are significantly lower than forces inside the ASNGs. They are close to Van der Waals forces by nature and depend on temperature significantly. In contrary to the bulk material, nanogrouping surface atoms fraction commensurates with their fraction inside. The presence of non-bridging surface oxygen atoms will lead to a negative microgroup charge. There are only calcium cations freely migrating in the molten matrix that can compensate this negative charge. Cations of calcium near the ASNGs surface will completely or at least partially compensate negative surface charge. An oxygen layer of the melt matrix behind the calcium cations compensates the positive  $\text{Ca}^{2+}$  surface layer charge. Therefore, the oxygen surroundings of  $\text{Ca}^{2+}$  will consist partially of the ASNG non-bridging oxygens, and also the molten matrix that provides large CN value of calcium by oxygen. Some anorthite crystal images from well-known collection of CIF-files for crystals and processed using Diamond 3-2 are shown in Fig. 10.

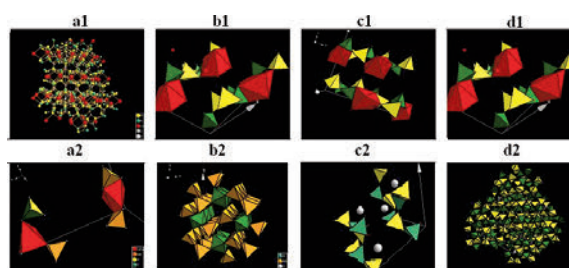


**Figure 10.** Crystalline structure of the anorthite: a1) silicon (yellow), aluminium (green), calcium atoms (red) in the anorthite lattice. b1, c1, d1, a2) - polyhedrons junction in the anorthite unit cell. Crystalline structure of the mullite: c2) silicon-oxygen and alumina-oxygen tetrahedra surrounded by  $\text{Ca}^{2+}$  (grey), d2) aluminium-oxygen tetrahedral network of one of the anorthite structures (calcium octahedrons are not shown)

As mentioned above, the short-range order in the melt retains some features of the short-range order of crystalline anorthite or mullite. During melting the formation of nanogroupings close to the regular polyhedrons of cluster type (for example, the Mackay cluster takes places). The regular polyhedron of cations and anions is formed under the action of powerful surface and electrostatic forces. These forces are responsible for spherically symmetric nanoclusters at the atomic grouping of small size [3]. The cluster has oxygen close packed structure. Octahedral and tetrahedral cavities are occupied with  $\text{Si}^{4+}$  and  $\text{Al}^{3+}$  cations with practically identical ionic radii. Slightly large cations (for example,  $\text{Al}^{3+}$ ) can also fill octahedral cavities.

A simplified model of the structure of anorthite or mullite melt is shown in Fig. 11. The figure shows only oxygen (yellow) and (red) calcium atoms. The ASNG is constructed on the principle of the Mackay cluster by cations  $\text{Al}^{3+}$  and  $\text{Si}^{4+}$ . In the case of anorthite, only tetrahedral cavities are occupied, and in the case of mullite, part of the octahedral cavities is occupied. Clusters of the smallest possible size can be present in disordered (quasi-gas) matrix. The cations  $\text{Si}^{4+}$ ,  $\text{Al}^{3+}$  are not shown, because the pattern is difficult to perceive.

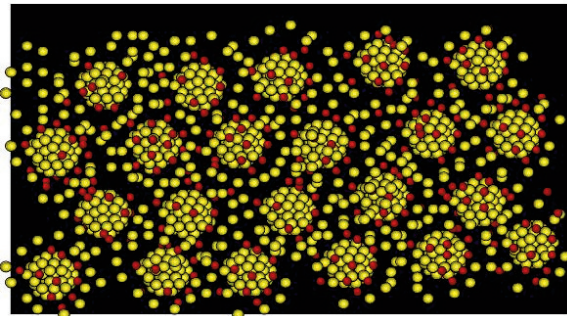


**Figure 11.** Model of the structure of anorthite or mullite melts based on close packed ASNG and quasi-gas matrix ( $\text{O}^{2-}$ - yellow balls,  $\text{Ca}^{2+}$  red balls).  $\text{Al}^{3+}$   $\text{Si}^{4+}$  cations are not shown

## 5. Conclusions

Anorthite and gehlenite demonstrated the absence of phase transitions in the temperature range between RT and melting point. The slight enlargement of lattice parameters with temperature rise was only detected. The features of aluminum-silicon-oxygen grid structure observed in anorthite crystals differ from the crystalline structure of eutectic samples studied in [6] that cause the difference in the aluminum-silicon-oxygen nanogroupings of the corresponding melts.

Silicon and aluminum are predominantly tetrahedrally coordinated by oxygen in the investigated melt. The interatomic Si - O and Al - O

distances in melts are consistent with those in crystals and melts of other oxide systems. Oxygen atoms form the nearest surroundings of  $\text{Ca}^{2+}$  at the distance of 0.223 nm with coordination number in the range between 8 and 10. It is evident that some distinctive structure elements of crystalline anorthite are retained in the anorthite melt.

Negatively charged ASNG are formed in investigated melts. This negative charge is compensated by  $\text{Ca}^{2+}$  cations that saturate the disordered (quasi-gas) matrix. The matrix consists of ions and small atomic clusters. The randomly distributed aluminum-silicon-oxygen nanogroups in the matrix resemble nanocrystals.

## References

- [1] V. Sokol'skii, A. Roik, A. Davidenko, V. Kazimirov, V. Lisniak, V. Galinich, I. Goncharov, J. Min. Metall. Sect. B-Metall., 48 (1) B (2012) 101-113.
- [2] E. Pastukhov, N. Vatolin, V. Lisin. et al., Diffraction studies of a structure of high-temperature melts, Ur. Div. Rus. Acad. Sci. Ekaterinburg, 2003, p.544.
- [3] N. Vatolin, E. Kern, V. Lisin, in Structure and physical-chemical properties of metallic and oxide melts, UNC AN USSR, Sverdlovsk, 1986, p.38-56.
- [4] E. Kern, I. Cherniavsky, L. Ziatkova, N. Vatolin, Glass Physics and Chemistry, 14 (1988) 182-186. In Russian.
- [5] E. Kern, I. Cherniavsky, L. Ziatkova, N. Vatolin, Glass Physics and Chemistry, 14 (1988) 206-212. In Russian.
- [6] V. Sokol'skii, D. Pruttskov, V. Busko, V. Kazimirov, O. Roik, A. Chyrkin, V. Galinich, I. Goncharov, J. Min. Metall., 54 (2) (2018) 133 - 141.
- [7] D. Pruttskov, V. Sokol'skii, E. Alekseev, V. Kazimirov, A. Roik, E. Vovchenko, Refractories and Technical Ceramics, 7-8 (2018) 3-12.
- [8] A.S. Berezhnoi, Multicomponent Alkali Oxide Systems, Naukova Dumka, Kiev, 1970, p. 458.
- [9] V. Sokol'skii, O. Roik, V. Kazimirov, in Advances in Materials Science Research V20: Nova Science Publishers, NY, 2015, p. 95-128.
- [10] V. Sokol'skii, V. Kazimirov, O. Roik et al., Welding Fluxes: Structural and Physicochemical Aspects of Slag Melts, PPC "The University of Kyiv", Kiev, 2015, p. 240
- [11] R.L. McGreevy, in Computer Modelling in Inorganic Crystallography (E. C Catlow), Academic Press, London, 1997, p.151 - 184.
- [12] A. Le Ball, J. Non-Cryst. Solids, 271 (2000) 249-259.
- [13] D. Keen, R. McGreevy, Nature, 344 (1990) 423-425.
- [14] A. Ilinskii, A. Romanova, L. Mikchailova et al., Metallofizika. 13 (2) (1991) 119-122.
- [15] J.R. Johnson, R.W. Bristow, H.H. Blau, J. Amer. Ceramic Soc. 34 (6) (1951) 165-172.
- [16] J. H. Welch, W. Gutt, J. Amer. Ceramic Soc., 42 (1) (1959) 11-15.
- [17] A.I. Zaitsev, B.M. Mogutnov, E.K. Shakhpazov, Physical Chemistry of Metallurgical Slag, Intercontact Science, Moscow, 2008, p 344.
- [18] R. Shannon, C. Prewit, Acta Crystallogr., B25 (5) (1976), 925-946.



## ISTRAŽIVANJE STRUKTURE TROJNIH JEDINJENJA $\text{CaO—Al}_2\text{O}_3\text{—SiO}_2$ U RASTOPLJNOM I KRISTALNOM STANJU UZ POMOĆ RENTGENSKE DIFRAKCIJE

V.E. Sokol'skii <sup>a</sup>, D.V. Pruttskov <sup>b</sup>, O.M. Yakovenko <sup>a</sup>, V.P. Kazimirov <sup>a</sup>, O.S. Roik <sup>a</sup>,  
N.V. Golovataya <sup>a</sup>, G.V. Sokolsky <sup>c</sup>

<sup>a</sup>\* Taras Ševčenko, Nacionalni univerzitet u Kijevu

<sup>b</sup> ZAO „Tehnokim“, Zaporozhje, Ukrajina

<sup>c</sup> Nacionalni tehnički univerzitet Ukrajine „Igor Sikorski Kijevski politehnički institut“

### Apstrakt

Kristalne strukture anortita i gelenita i uređenost kratkog dometa rastopljenog anortita proučavane su uz pomoć rentgenske difrakcije u rasponu od sobne temperature pa do ~ 1923 K. Identifikovane su korespondirajuće faze anortita i gelenita kao i amorfna komponenta uzoraka anortita koji su imali identičan oblik kao i XRD uzorak rastopljenog anortita. Faktorska struktura i radijalna distribuciona funkcija atoma rastopljenog anortita izračunate su iz eksperimentalnih podataka dobijenih visokotemperaturnom rentgenskom difrakcijom. Parcijalni strukturni parametri uređenosti kratkog dometa rastopa rekonstruisani su pomoću reverzne Monte Karlo simulacije.

**Ključne reči:** Gelenit; Anortit; Mulit; Visokotemperaturna rentgenska difrakcija; RMC simulacije

